Broadband subwavelength focusing of light using a passive sink

Heeso Noh[1,2] **Sébastien M. Popoff**[1] **and Hui Cao**[1,*]

[1] *Department of Applied Physics, Yale University, New Haven, CT 06520, USA*
[2] *Department of Nano and Electronic Physics, Kookmin University, Seoul, South Korea*

[*] *hui.cao@yale.edu*

Abstract: Optical absorption is usually considered deleterious, something to avoid if at all possible. We propose a broadband nanoabsorber that completely eliminates the diffracting wave, resulting in a subwavelength enhancement of the field. Broadband operation is made possible by engineering the dispersion of the complex dielectric function. The local enhancement can be significantly improved compared to the standard plane wave illumination of a metallic nanoparticle. Our numerical simulation shows that an optical pulse as short as 6 fs can be focused to a 11 nm region. Not only the local field, but also its gradient are greatly enhanced, pointing to applications in ultrafast nonlinear spectroscopy, sensing and communication with deep-subwavelength resolution.

© 2013 Optical Society of America

OCIS codes: (030.0030) Coherence and statistical optics; (240.0240) Optics at surfaces.

References and links

1. R. Carminati, R. Pierrat, J. de Rosny and M. Fink, "Theory of the time reversal cavity for electromagnetic fields," Opt. Lett. **32**, 3107–3109 (2002).
2. J. de Rosny and M. Fink, "Overcoming the diffraction limit in wave physics using a time-reversal mirror and a novel acoustic sink," Phys. Rev. Lett. **89**, 124301 (2002).
3. P. Kinsler, "Active drains and causality," Phys. Rev. A **13**, 055804 (2011).
4. Y. G. Ma, S. Sahebdivan,C. K. Ong, T. Tyc and U. Leonhardt, "Evidence for subwavelength imaging with positive refraction," New J. Phys. **13**, 033016 (2002).
5. Y. D. Chong, L. Ge, H. Cao, and A. D. Stone, "Coherent perfect absorbers: Time-reversed lasers," Phys. Rev. Lett. **105**, 053901 (2010).
6. W. Wan, Y. Chong, L. Ge, H. Noh, A. D. Stone, and H. Cao, "Time-reversed lasing and interferometric control of absorption," Science **331**, 889–892 (2011).
7. H. Noh, Y. Chong, A. D. Stone, and H. Cao, "Perfect coupling of light to surface plasmons by coherent absorption," Phys. Rev. Lett. **108**, 186805 (2012).
8. G. Montaldo, G. Lerosey, A. Derode, A. Tourin, J. de Rosny, and M. Fink, "Telecommunication in a disordered environment with iterative time reversal," Waves in Random Media **14**, 287–302 (2004).
9. M. Pu, Q. Feng, M. Wang, C. Hu, C. Huang, X. Ma, Z. Zhao, C. Wang, and X. Luo, "Ultrathin broadband nearly perfect absorber with symmetrical coherent illumination," Opt. Express **20**, 2246–2254 (2012).
10. A. Wicht, K. Danzmann, M. Fleischhauer, M. Scully, G. Müller, and R. H. Rinkleff, "White-light cavities, atomic phase coherence, and gravitational wave detectors," Opt. Commun. **134**, 431–439 (1997).
11. N. Yang and A. E. Cohen, "Local geometry of electromagnetic fields and its role in molecular multipole transitions," J. Phys. Chem. B **115**, 5304–5311 (2011).
12. P. A. Belov, C. R. Simovski, and S. A. Tretyakov, "Example of bianisotropic electromagnetic crystals: The spiral medium," Phys. Rev. E **67**, 056622 (2003).
13. A. I. Rahachou and I. V. Zozoulenko, "Light propagation in nanorod arrays," J. Opt. A: Pure and Applied Optics **9**, 265–270 (2007).
14. N. Fang, D. Xi, J. Xu, M. Ambati, W. Srituravanich, C. Sun, and X. Zhang, "Ultrasonic metamaterials with negative modulus," Nat. Mater. **5**, 452–456 (2006).

15. C. Ding, L. Hao, and X. Zhao, "Two-dimensional acoustic metamaterial with negative modulus," J. Appl. Phys. **108**, 074911 (2010).

1. Introduction

Overcoming the diffraction limit and focusing waves on a deep-subwavelength scale have been widely pursued for light, microwave and acoustics. The tight focusing not only can strongly enhance linear and nonlinear interactions between waves and matter, but also greatly improve the spatial resolution in sensing, imaging and communication. It is well known that in a homogeneous medium, wave diffraction limits the size of a focal spot to half the wavelength. This limit can be understood in a simple case of a monochromatic scalar wave. Consider a spherical wave $e^{-ikr-i\omega t}/r$ converging to the origin $r = 0$, where ω is the angular frequency, $k = 2\pi/\lambda$ and λ is the wavelength. After passing the origin, the wave becomes diverging, of the form $e^{ikr-i\omega t}/r$. The total field is a superposition of the two, i.e, $e^{ikr-i\omega t}/r - e^{-ikr-i\omega t}/r \propto \sin(kr - \omega t)/r$, which is proportional to the imaginary part of Green's function [1] - the solution to the wave equation in a homogeneous medium. The minus sign of the diverging wave causes a destructive interference of the incoming and outgoing waves, which removes the singularity at $r = 0$. The focal spot has a width of $\pi/k = \lambda/2$, the well-known diffraction limit. Therefore, diffraction is a consequence of destructive interference of the converging and diverging waves.

One way of breaking the diffraction limit is to make the interference constructive by flipping the sign of outgoing wave, so that the total field becomes $e^{ikr-i\omega t}/r + e^{-ikr-i\omega t}/r \propto \cos(kr - \omega t)/r$. This can be done by placing a resonant scatterer at the origin. Below the resonant frequency, the diffracted wave experiences a π phase shift. For the visible light, the surface plasmon resonance of a metallic nanosphere might be used. The intrinsic absorption of metal, however, would weaken the interference effect.

An alternative is to utilize the absorption to eliminate the outgoing wave, so the total field is equal to the incoming one $e^{ikr-i\omega t}/r$. This can be realized by placing a perfect absorber at the origin. The field amplitude, albeit a factor of two smaller than in the first case, approaches infinity as $r \to 0$. Diffraction is thus overcome, as demonstrated by de Rosny and Fink in an acoustic wave experiment [2]. They used a time-reversed sink to cancel the diffracted wave $e^{-ikr-i\omega t}/r$ and obtained a focal spot smaller than $\lambda/14$. This active sink can operate over a broad frequency range, but it requires prior knowledge of the incoming signal [3] and a setup to generate the time reverse source at the focal spot. The idea of using a sink to remove the diverging wave has recently been extended to microwaves [4].

In this paper, we propose a passive sink which is not driven externally and does not need prior knowledge of the temporal profile of the impinging wave. This method is based on the coherent perfect absorber we recently developed [5–7]. Perfect absorption of coherent light by two- or three-dimensional metallic nanostructures can be achieved via critical coupling to surface plasmon resonances [7]. Although it was originally demonstrated for narrow-band operation, we will show here that nearly perfect absorption can be realized over a continuous band of frequency by engineering the dispersion of the complex dielectric function. We demonstrate in numerical simulation that a 6.7 fs pulse is focused from far field to a region of ~ 13 nm. The temporal shape of the pulse can be arbitrary; as long as the spatial wavefront matches the time-reversed radiation pattern of a surface plasmon resonance, the incident pulse will be completely absorbed.

The nearly perfect absorption of an ultrashort optical pulse results in strong localization of the electric field energy in space and time, which greatly enhances light-matter interactions, e.g., two-photon excitation of molecules. Not only the field amplitude but also the field gradient is enhanced by many orders of magnitude, when the incoming light is critically coupled to a multipole resonance of surface plasmon in the metallic nanoparticle. The steeply varying

field can efficiently excite the dipole-forbidden transitions of molecules and probe the dark states. Hence, the broad-band nearly perfect absorber may be useful for ultrafast nonlinear spectroscopy and sensing at the nanoscale. Furthermore, our scheme is general and applicable to other types of waves, e.g. acoustic wave, microwave, pointing to possible applications in shock wave lithotripsy, microwave communication with deep-subwavelength resolution [8]. The nearly perfect absorption of an ultrashort optical pulse results in strong localization of the electric field energy in space and time, which greatly enhances light-matter interactions, e.g., two-photon excitation of molecules. Not only the field amplitude but also the field gradient is enhanced by many orders of magnitude, when the incoming light is critically coupled to a multipole resonance of surface plasmon in the metallic nanoparticle. The steeply varying field can efficiently excite the dipole-forbidden transitions of molecules and probe the dark states. Hence, the broad-band nearly perfect absorber may be useful for ultrafast nonlinear spectroscopy and sensing at the nanoscale. Furthermore, our scheme is general and applicable to other types of waves, e.g. acoustic wave, microwave, pointing to possible applications in shock wave lithotripsy, microwave communication with deep-subwavelength resolution [8].

2. Principle

In principle, if a subwavelength object is placed at $r = 0$, the outgoing wave can undergo a phase shift and its amplitude may be reduced. This two effects are respectively due to the internal resonance and dissipation of the object. The destructive interference effect cancels the diverging part of the field only when the incoming and outgoing waves have the same amplitude and π phase difference. Any deviation from these conditions leads to a subwavelength enhancement of the field. That is why the commonly used plane wave illumination of a metallic nanoparticle, that is dissipative and has resonance close to the optical excitation wavelength, produces a strong local field enhancement. In the introduction section we discussed two extreme scenarios to optimize the subwavelength field enhancement: adjusting only the amplitude or the phase of the outgoing wave. In this section, we will consider more general cases.

First, we show how to change the relative phase between the converging and diverging waves to make them interfere constructively. For simplicity, we limit our analysis to two-dimensional (2D) waves, the extension to 3D is straight-forward [7]. Let us consider a cylindrical wave propagates in the $x - y$ plane towards the origin; its magnetic field is along the z axis. After converging at the origin, the wave diverges, and the total field can be written in the polar coordinates as $H_z(r,\theta) = H_m^{(2)}(kr)e^{im\theta} + sH_m^{(1)}(kr)e^{im\theta}$, where $H_m^{(1)}$ ($H_m^{(2)}$) is the mth-order Hankel function of the first (second) kind and represents an outgoing (incoming) wave. The complex number, s, is the relative amplitude of the outgoing wave; in the absence of dissipation the outgoing wave carries the same energy as the incoming wave, $|s| = 1$. The phase of s is determined by the solution to the Maxwell's equations, which gives $s = 1$ in vacuum or lossless dielectric media. Although both $H_m^{(1)}(kr)$ and $H_m^{(2)}(kr)$ diverge at $r = 0$, the total field remains finite, because the diverging part of $H_m^{(1)}(kr)$ is canceled by that of $H_m^{(2)}(kr)$. This cancellation can be regarded as a consequence of destructive interference between the incoming and outgoing waves.

To switch to constructive interference, we must reverse the sign of s. One way is placing a cylinder of radius R at $r = 0$ to interact with the incident wave. Due to the cylindrical symmetry of the system, the angular momentum m is conserved upon scattering, so is the polarization. Thus the total field outside the cylinder ($r > R$) has the same expression as before, but with a different value of s; inside the cylinder ($r < R$) $H_z(r,\theta) = aJ_m(nkr)e^{im\theta}$, where J_m is the Bessel function of the first kind, $n = \sqrt{\varepsilon}$, ε is the complex dielectric function of the cylinder, and a is a normalization constant. By matching the fields at the cylinder surface ($r = R$), we solve for s and get $s =$

$[nJ_m(nkR)H_m^{(2)'}(kR) - J'_m(nkR)H_m^{(2)}(kR)]/[J'_m(nkR)H_m^{(1)}(kR) - nJ_m(nkR)H_m^{(1)'}(kR)]$, where J' (H') is the first-order derivative of the Bessel (Hankel) function. In the following, we will consider three different situations: a metallic nanoparticle illuminated by a plane wave (Fig. 1(a)), the same object illuminated by a cylindrical wave that matches a resonant mode of the particle (Fig. 1(b)) and a cylindrical wave in an homogeneous medium (Fig. 1(c)).
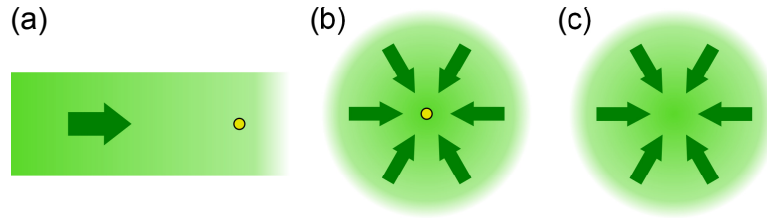

Fig. 1. Different configurations studied. (a) a nanoparticle illuminated by a plane wave. (b) a nanoparticle illuminated by a cylindrical wave. (c) cylindrical wave in an homogeneous medium.

Setting $s = -1$ for a particular m, we find the complex ε if k and R are fixed. Alternatively, we can fix ε and solve for k and R. Figure 2 shows the dipole ($m = 1$) and quadrupole ($m = 2$) solutions for a cylinder of $R = 5.1$ nm. The wavelength λ of light in the vacuum outside the cylinder is set at 532 nm. In both cases, the imaginary part of ε (ε_i) vanishes, the cylinder has no loss and $|s| = 1$. ε is purely real and negative, representing a lossless metal. In the quasi-static limit, surface plasmon resonances occur at $\varepsilon = -1$. Below the resonant frequency (where ε is slightly less than -1), the outgoing wave experiences an additional π phase shift, and $s = -1$. The diverging parts of $H_m^{(1)}(kr)$ and $H_m^{(2)}(kr)$ no longer cancel each other giving rise to huge local field enhancements commonly observed with metallic nanoparticles.

The total field does not diverge due to the finite radius and reaches the maximal value at the surface of the cylinder ($r = R$). The smaller the R, the larger the maximal field magnitude. As shown in Fig. 2, the electric field intensity at $r = R$ is 10^5 times higher than what can be obtained by focusing in vacuum without the cylinder for $m = 1$. Nevertheless, a similar enhancement is obtained by exciting the same particle with a plane wave. When $kR \ll 1$, the input energy is predominantly coupled to the $m = 1$ mode that has the lowest quality factor and whose radiation pattern has a better overlap with the plane wavefront. The enhancement originates from the same dipole resonance, thus the behavior is similar. However, for $m = 2$, the field enhancement at $r = R$ is 1.5×10^9, which is about 3 times that with plane wave excitation. The quadrupole resonance ($m = 2$) has stronger field enhancement, because of its lower radiative decay rate and higher quality factor. Since the plane wave excitation couples most of the input energy into the $m = 1$ resonance that has a lower quality factor than the $m = 2$ resonance, the field enhancement is weaker than that with a cylindrical wave of $m = 2$. Excitation of higher-order ($m > 2$) resonances will lead to a further enhancement of local fields.

To describe the size of the focal spot, we use the effective diameter defined as $d_{eff} = 2\int_0^\infty (|E_r|^2 + |E_\theta|^2)r^2 dr / \int_0^\infty (|E_r|^2 + |E_\theta|^2)r dr$. In Fig. 1, $d_{eff} = 18$ nm for $m = 1$, and $d_{eff} = 11$ nm for $m = 2$. These value are approximately $\lambda/40$. Without the cylinder, the effective diameter of the focal spot is 212 nm, close to $\lambda/2$ - the diffraction limit. In fact, the focal spot size, which is slightly larger than the diameter of the cylinder (10.2 nm), can be further reduced by using a smaller cylinder. However, the value of ε_r must be set correctly. As shown in Fig. 3(a), a slight deviation of ε_r from the right value makes s a complex number. The phase relation between the incoming and outgoing waves is modified, and they no longer interfere constructively. The total field can be expressed as the sum of a diverging term and a non-diverging
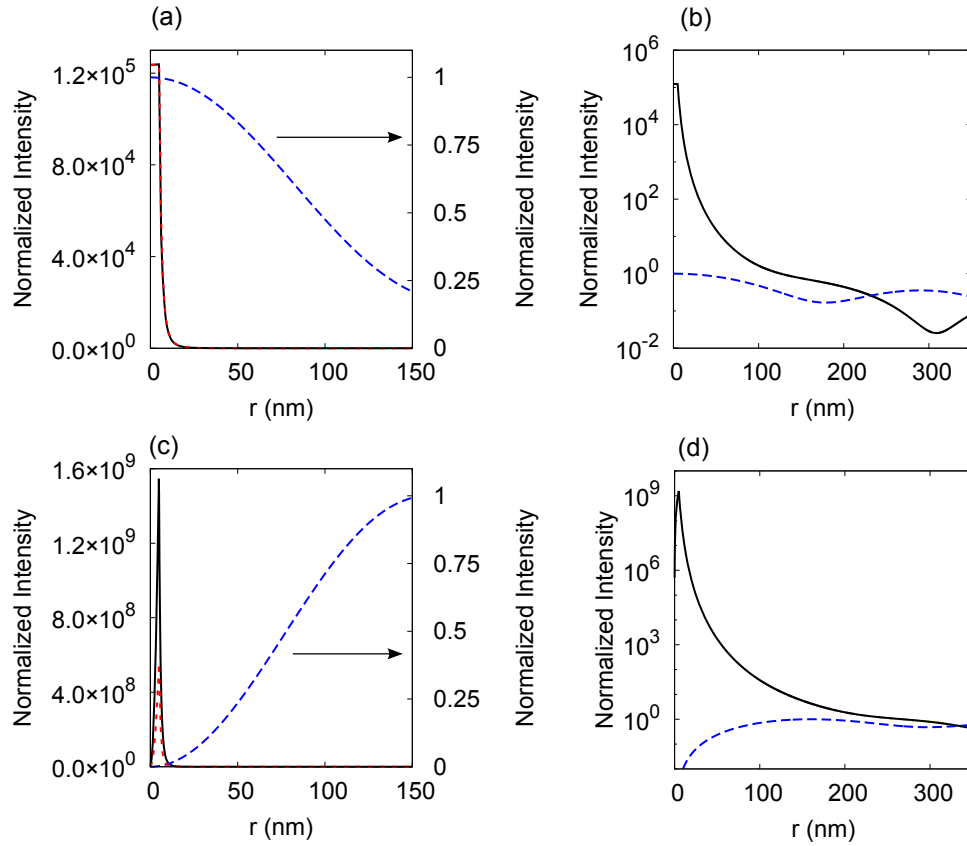
Fig. 2. Interference between a focusing wave ($\lambda = 532$ nm) and its diffracted wave is made constructive ($s = -1$) by placing a lossless metallic nanoparticle ($R = 5.1$ nm; $\varepsilon = -1.01$ for $m = 1$; $\varepsilon = -1.001$ for $m = 2$) at the origin ($r = 0$). Black solid curves (blue dashed curves) represent the radial distributions of electric field intensity with (without) the metallic scatterer for $m = 1$ (a,b) and $m = 2$ (c,d) in the linear scale (a,c) and the logarithmic scale (b,d). For comparison, the red dotted curves in (a,c) are the intensities when a plane wave is incident onto the metallic scatterer. All the intensities are normalized to the maximal values that can be obtained by focusing the same incident waves in vacuum without the particle. Maximal local field intensities are enhanced 5 orders of magnitude for $m = 1$ and 9 orders of magnitude for $m = 2$.
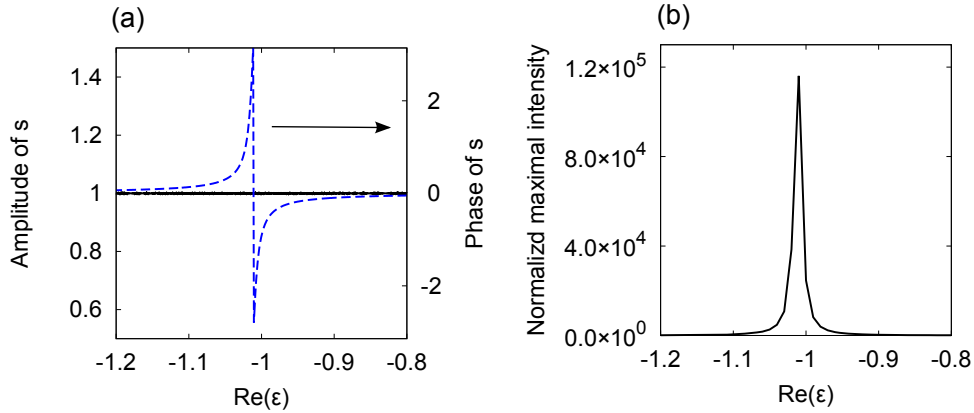
(a) (b)

Fig. 3. (a) Relative amplitude (black solid line) and phase (blue dashed line) of the diffracted wave s ($\lambda = 532$ nm, $m = 1$) as a function of the real part of the dielectric constant ε of the metallic cylinder ($R = 5.1$ nm). As soon as the value of Re[ε] deviates from that for $s = -1$, the phase of s changes dramatically, breaking the condition for constructive interference of the scattered wave and the incident wave. (b) Maximal electric field intensity I_e at the cylinder surface ($r = R$) as a function of the real part of ε. I_e is normalized to the maximal field intensity produced by the same incident wave in the absence of the cylinder. When s deviates from -1, I_e drops quickly.

term, $H_z(r, \theta) = H_{ND}(r, \theta) + (1 - s)H_D(r, \theta)$, with $H_{ND}(r, \theta) = H_m^{(2)}(kr)e^{im\theta} + H_m^{(1)}(kr)e^{im\theta}$ and $H_D(r, \theta) = H_m^{(1)}(kr)e^{im\theta}$. As s deviates from 1, the maximal field intensity drops quickly [Fig. 3(b)].

To achieve $s = -1$, the metallic nanocylinder must be lossless ($\varepsilon_i = 0$), which is difficult to realize at optical frequency. What happens if $\varepsilon_i \neq 0$? Figure 4(a) shows how the amplitude and phase of s change as we fix ε_r and gradually increase ε_i for $m = 1$. At small ε_i, the amplitude of s drops, while the phase stays nearly constant. Hence, the absorption merely reduces the amplitude of the outgoing wave, but does not change its phase relation to the incoming one. The two waves still interfere constructively, albeit not as strongly as in the lossless case and the maximal field intensity decreases [Fig. 4(b)]. When ε_i reaches a critical value 5.72×10^{-3}, $s = 0$, the outgoing wave vanishes, the incoming wave is completely absorbed via critical coupling to the nanocylinder cavity. With a further increase of the ε_i, the outgoing wave reappears, but with a π phase shift. The interference between the incoming and outgoing waves becomes destructive, causing a further reduction of the maximal field intensity. The local field enhancement is determined by the diverging term of the total field, whose intensity is proportional to $|1 - s|^2$, which fits well the maximal intensity in Fig. 3(b). Since the destructive interference effect cancels the diverging part of the field only when s is very close to 1, the spot size is otherwise mainly governed by the huge local field enhancement close to the metallic surface. Nevertheless, as the imaginary part of ε increases, the relative weight of the diverging term decreases and the effective diameter of the focal spot gradually increases in Fig. 4(b).

In the above calculation we used the cylindrical wave that perfectly matches the radiation pattern of the resonance of a nanocylinder. If the incident beam is not a full cylindrical wave, it can be expressed as a linear superposition of multiple cylindrical waves of different azimuthal number m. Since only some of these components can meet the condition for perfect absorption, the local field enhancement and sub-diffractcion focusing are still present but weaker than the cases shown above.
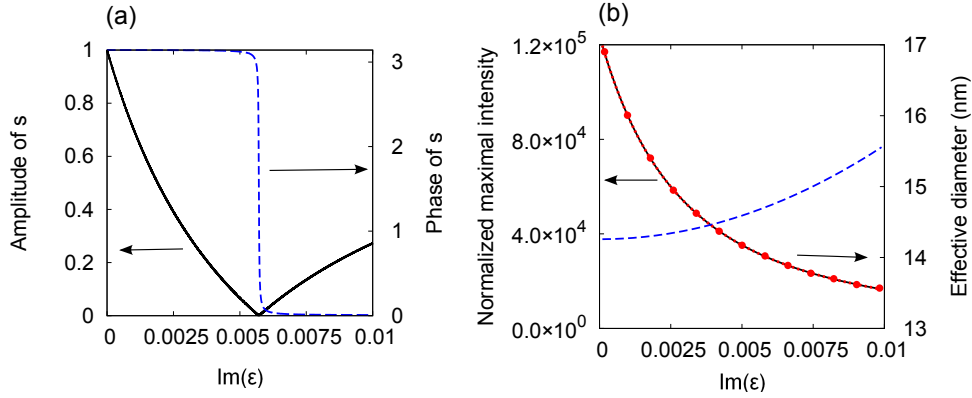
Fig. 4. (a) Relative amplitude (black solid line) and phase (blue dashed line) of the diffracted wave s ($\lambda = 532$ nm, $m = 1$) as a function of the imaginary part of the dielectric constant ε of the metallic cylinder ($R = 5.1$ nm). The real part of ε is fixed at -1.01. As the amplitude of s reaches zero, its phase experiences a π shift. (b) Maximal electric field intensity I_e at the cylinder surface (black solid line) and the focal spot size defined by the effective diameter d_{eff} (blue dashed line) as a function of the imaginary part of ε. I_e is normalized to the maximal field intensity produced by the same incident wave in the absence of the cylinder. The red dotted curve represents the fit $I_e = \alpha \left|1 - s\right|^2$, with $\alpha = 6.19 \times 10^4$. As the imaginary part of ε increases from 0 to 0.01, I_e decreases monotonically, while the effective spot size increases
.

3. Broadband response

The above study was performed at a single frequency. Is it possible to achieve subwavelength focusing for a broad-band pulse? To answer this question, let us consider the case $s = 0$; the solution can be easily extended to other values of s. $s = 0$ corresponds to the perfect absorption of the incoming wave, which has been studied previously for narrow-band operation [7]. It utilizes critical coupling to the surface plasmon resonances in metallic nanostructures to achieve complete absorption. Since the surface plasmon resonances exist at discrete frequencies, the perfect absorption is narrow-band. Recently, an one-dimensional broad-band nearly perfect absorber was proposed and simulated by utilizing dispersive materials, e.g. the heavily doped silicon [9].

To design a passive sink of subwavelength size for a broad frequency range is not trivial because of causality. The causality of a physical system implies that the complex dielectric function must be analytic in the upper half of the complex plane. The scattering matrix, that links the incoming eld to the outgoing eld, should also be an analytic function in the upper half-plane. A consequence is that the amplitude of the outgoing eld can only be zero at discrete frequencies. Aware of this limitation, we will rst nd the mathematical solution for the complex dielectric function corresponding to $s = 0$ in a broad frequency range. We then use the Lorentz model, that satises the analyticity of the dielectric function, to approximate this solution.

We consider a nanocylinder of $R = 5.1$ nm. We calculate the complex ε for satisfying $s = 0$ at each wavelength λ in the range of 456 nm to 638 nm. Figure 5 plots ε_r and ε_i versus $k = 2\pi/\lambda$ for $m = 1$. As k increases, ε_r decreases, and ε_i increases. Such dispersion can be realized at the low frequency side of a material resonance. We fit the dispersive ε by the Lorentz model:

$$\varepsilon^{(f)}(\omega) = \varepsilon_{\text{inf}} - \frac{\omega_p^2}{\omega^2 - \omega_0^2 + i\omega\Gamma_0}, \tag{1}$$

where ω_0 is the resonant frequency, Γ_0 is the damping constant, ω_p is the plasma frequency,

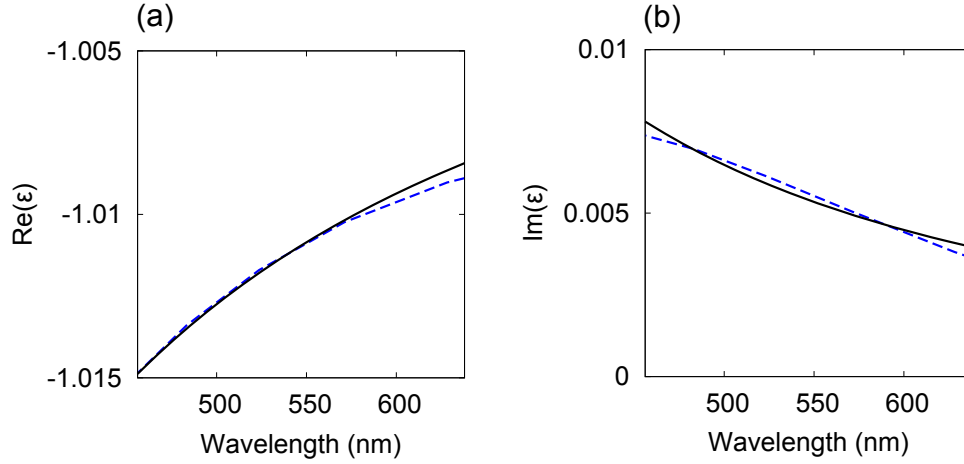ε_{inf} is the non-resonant high-frequency component of the dielectric function.

Fig. 5. Black solid curves in (a) and (b) are the real and imaginary parts of the dielectric function ε of a nanocylinder ($R = 5.1$ nm) at $r = 0$ for perfect absorption of a cylindrical wave ($m = 1$) at every wavelength in the range of 456 nm - 638 nm. The blue dashed curves represents the best fitting of complex dielectric function with the Lorentz model descried by Eq. (1). The parameters are given in the text.

The dashed lines in Fig. 5(a,b) shows the best fit with $\omega_0 = 5.28 \times 10^{15}$, $\omega_p = 6.67 \times 10^{14}$, $\Gamma_0 = 5.85 \times 10^{15}$ and $\varepsilon_{\text{inf}} = -1.02 + 0.008i$. Such a dispersion relation, the cylinder can nearly perfectly absorb the incoming waves $H_{m=1}^{(2)}(kr)$ across the wavelength range of 456 nm - 638 nm. Thus it can be considered as a "white-light" nanocavity, in analog to the macroscopic white-light cavities utilizing the negative dispersion of atoms [10].

The broadband operation enables a nearly perfect absorption of a short pulse that is spread over the wavelength range of 456 nm - 638 nm. Figure 6(a) and (b) are movies (online) showing the temporal evolution of the field distribution when a Gaussian pulse of width 6.7 fs is impinging on the cylinder. The magnetic field of the incident pulse is $H_z = H_m^{(2)}(kr)e^{im\theta}f(t)$, where $f(t) = e^{(t+r/c)^2/3.3^2}e^{-i\omega_c t}$, t is in the unit of femtosecond, ω_c is $2\pi c/\lambda$ ($\lambda = 532$ nm) and c is velocity of light. The incident wave has an angular momentum $m = 1$ ($m = 2$) in Fig. 6(a) [(b)], exciting the dipole (quadruple) resonance of the surface plasmon in the nanocylinder. In either case, the incoming pulse is completely absorbed by the cylinder, resulting in a nanoscale focal spot. Consequently, a strong local field builds up in the vicinity of the cylinder for a short period of time. Figure 6(b) plots the temporal evolution of the electric field intensity at the cylinder surface $I_e(r = R, t)$. It shows a peak of width 6.7 fs, equal to the incident pulse width. The peak height is 4 (8) orders of magnitude higher than the focused intensity of the same pulse without the cylinder for $m = 1$ ($m = 2$). As a comparison, we plot the temporal response of a non-dispersive particle that satisfies $s = 0$ for $m = 1$ at the central frequency of the pulse. The maximal amplitude of the pulse is 3.3 times weaker than that with the tailored dispersive particle. The focal spot size is $d = 18$ nm, 11 nm for $m = 1, 2$. Therefore, the nanocylinder with an appropriate dispersion $\varepsilon(\lambda)$ enables the deep-subwavelength focusing of a broadband signal, that greatly enhances the local fields.

Note that with the same dispersive ε, optical pulses of arbitrary temporal shape can be completely absorbed, as long as all the spectral components are within the bandwidth of nearly perfect absorption. We repeat the calculation with chirped pulses, and the incident wavefront remains cylindrical. Figure 6(d) is a movie of a pulse with the chirped temporal form
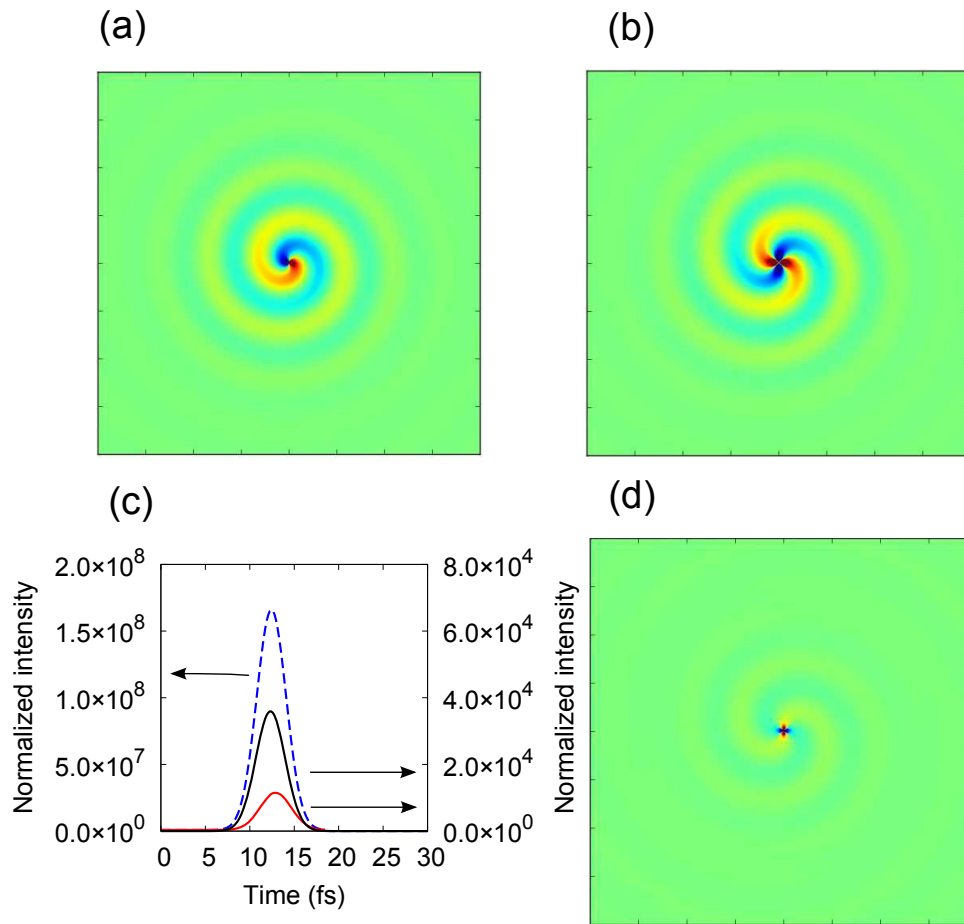
Fig. 6. (a,b) Single-frame excerpts from movies (Media 1, Media 2) of the spatial distribution of magnetic field $H_z(r,\theta)$ when a Gaussian pulse of width 6.7 fs impinges on a nanocylinder ($R = 5.1$ nm) at the origin ($r = 0$). The pulse has a cylindrical wavefront and an angular momentum $m = 1$ in (a), $m = 2$ in (b). The pulse spectra is centered at $\lambda = 532$ nm with a FWHM of 180 nm. The dispersive dielectric function of the nanocylinder is chosen to reach a nearly perfect absorption at all incident wavelengths. (c) Electric field intensity at the surface of the cylinder ($r = R$) as a function of time in the case of (a) - black solid line, and (b) - blue dashed line. The red curve represents the field intensity when the dielectric function is non-dispersive and perfect absorption is reached only at the center wavelength $\lambda = 532$ nm of the incident pulse for $m = 1$. The intensity is normalized by the maximal intensity of the same incident pulse without the nanocylinder. (d) Single-frame excerpts from movies showing a chirped pulse (Media 3), whose spectrum and spatial wavefront are identical to the Gaussian pulse in (b), is nearly perfectly absorbed by the nanocylinder with the same $\varepsilon(\lambda)$. The temporal profile of the pulse is described in the text.

$f(t) = e^{(t+r/c)^2/3.3^2} e^{-i(\omega_c - 0.55t)t}$, t in the unit of fs, and $m = 2$ impinging on the nanocylinder. The pulse is focused to a $\lambda/44$ spot via nearly perfect absorption of the diffracted wave.

We note that the broadband subwavelength absorber is not a blackbody. The difference is that the blackbody can perfectly absorb light incident from any direction with arbitrary wavefront, while the near-perfect absorber works only for specific wavefront of the incident light.
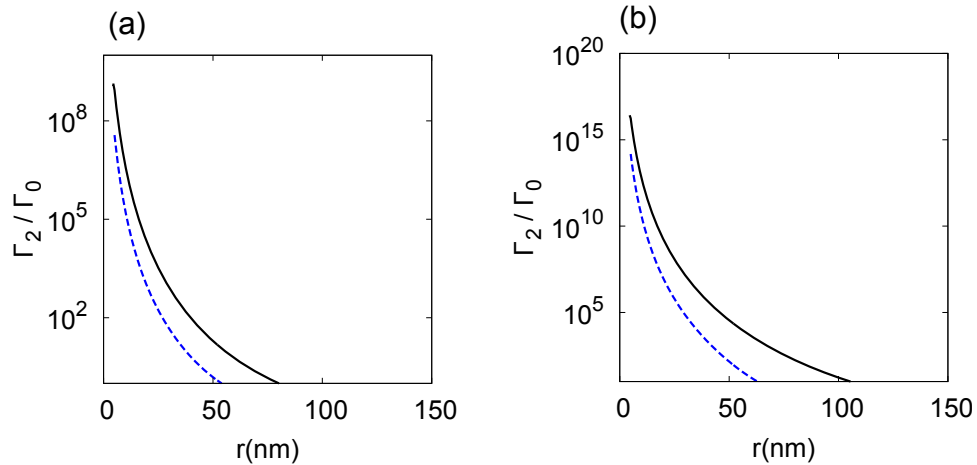

Fig. 7. Two-photon excitation rate Γ_2 as a function of the radial coordinate r when a Gaussian pulse of width 6.7 fs is nearly perfectly absorbed by a nanocylinder ($R = 5.1$ nm) at $r = 0$. The incident pulse has the cylindrical wavefront of $m = 1$ in (a), $m = 2$ in (b) (black solid line). For comparison, the dashed blue curve represents the incident wave of a plane front. The pulse spectra and the dielectric function of the cylinder in (a) and (b) are identical to those in Fig. 6(a) and (b), respectively. Γ_2 is normalized by the maximal two-photon excitation rate Γ_0 of the same input pulse without the nanocylinder.

4. Applications

The subwavelength focusing of a short optical pulse greatly enhance the local field, which may be utilized to enhance the light matter interaction, especially the nonlinear one. As an example, we consider the two-photon excitation of molecules in the vicinity of a metallic nanocylinder ($R = 5.1$ nm) under the condition of broadband nearly perfect absorption. The rate of two-photon excitation by a short pulse at a spatial position (r, θ) is $\Gamma_2(r, \theta) \propto \int I_e^2(r, \theta, t)dt$, where I_e is the electric field intensity. Due to the cylindrical symmetry of the system and the excitation wave, Γ_2 is independent of θ. Figure 7 plots the enhancement of Γ_2, i.e. the ratio $\Gamma_2(r)/\Gamma_0$, where Γ_0 is the maximal rate of local two-photon excitation by the same incident pulse in the absence of the nanocylinder. At the cylinder surface, $\Gamma_2/\Gamma_0 = 10^9$ for $m = 1$, and 3×10^{16} for $m = 2$. These enhancements are respectively 30 and 300 times higher than the ones obtained with the same short pulse having a plane wavefront ($\Gamma_2/\Gamma_0 = 3 \times 10^7$ and 10^{14}). Such enhancements occurs only locally ($r = R$). Moving away from the cylinder surface, Γ_2 decreases rapidly. The spatially-integrated rate, $\Gamma_{2t} = 2\pi \int_R^\infty \Gamma_2(r)rdr$, is proportional to the total intensity of fluorescence from two-photon excitation. After normalizing it by that without the cylinder, we obtain the total enhancement factor, which is 9.7×10^7 for $m = 1$, and 8.1×10^{15} for $m = 2$. The enhancement factor can be further increased by using higher-order resonances ($m > 2$) or smaller scatterers ($R < 5$ nm).

In addition to the field amplitude, the field gradient is also greatly enhanced. The steeply varying electric field can efficiently excite molecular multipole transitions that are barely ex-
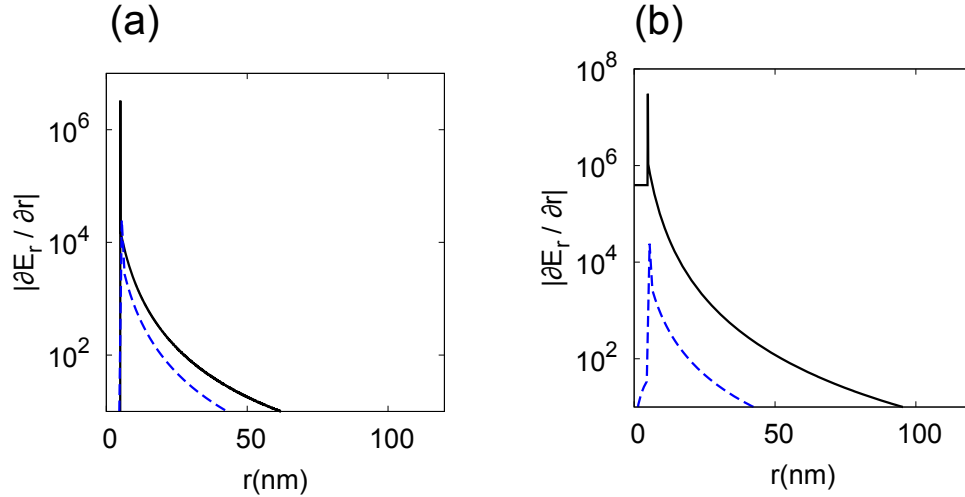
Fig. 8. Radial gradient of the electric field component in the radial direction E_r, in the case a cylindrical wave nearly perfectly absorbed by a nanocylinder ($R = 5.1$ nm) located at $r = 0$ (black solid line) and a plane wave excitation of the same cylinder (dashed blue line) at $\lambda = 532$ nm. $m = 1$ in (a), $m = 2$ in (b). $|\partial E_r/\partial r|$ is normalized by the maximal gradient without the nanocylinder.

cited, if at all, by far-field plane waves. For example, the rate of electric quadrupole transition is proportional to the spatial gradient of the electric field [11]. As an illustration, we calculate the electric field gradients in the case of perfect absorption at a single wavelength $\lambda = 532$ nm. For the TM-polarized light, the electric field has the radial component $E_r(r, \theta)$ and the azimuthal component $E_\theta(r, \theta)$. There are four gradients, among them the radial gradient of E_r has the largest amplitude. Figure 8 compares $|\partial E_r/\partial r|$ with a $R = 5.1$ nm cylinder to that without for $m = 1$ [Fig. 8(a)] and $m = 2$ [Fig. 8(b)]. At the cylinder surface, $|\partial E_r/\partial r|$ reaches the maximal value, which is seven (six) orders of magnitude higher for $m = 2$ ($m = 1$) than the maximal value without the cylinder. By comparison, a plane wave excitation at the same wavelength gives rise to an enhancement of four orders of magnitudes lower in both cases. Such a dramatic enhancement of the field gradient will lead to an efficient excitation of the multiple transitions.

5. Conclusion

In summary, we have proposed and simulated a broadband passive sink that can greatly improve the subwavelength focusing with a nanoparticle. It relies on the coherent absorption to eliminate the outgoing (diverging) wave, which would otherwise interfere with the incoming (converging) wave to produce the diffraction pattern that limits the spatial resolution.

The sink is not driven externally, and a broadband operation is made possible by engineering the dispersion of the complex dielectric function. Our numerical simulation shows that an optical pulse as short as 6 fs can be focused to a 11 nm region. This scheme can be easily extended to microwave and acoustic wave. The spectral dispersion for broadband response is reachable with carefully-designed metamaterials [12–15]. Such metamaterials based on deep subwavelength resonators can both have a tailored dispersion relation and a size smaller than the wavelength. This media are good candidates for the fabrication of subwavelength nearly perfect absorbers for microwave and acoustic wave.

The broadband nearly perfect nanoabsorber enables deep-subwavelength focusing of short optical pulses, which will greatly enhance nonlinear optical process. The spatial gradient of

the field will also be enhanced dramatically, which may efficiently excite the dark states of molecules. Potential applications include ultrafast nonlinear spectroscopy, sensing and communication with deep-subwavelength resolution.

Acknowledgments